Computers & Structures Vol. 38, No. 2, pp. 239–246, 1991
Printed in Great Britain.

0045-7949/91 $3.00 + 0.00
Pergamon Press plc

A FINITE ELEMENT FOR MODELING DELAMINATIONS IN COMPOSITE BEAMS

B. V. SANKAR
Department of Aerospace Engineering, Mechanics and Engineering Science, University of Florida, Gainesville, FL 32611, U.S.A.

(*Received* 17 *August* 1989)

Abstract—A shear deformable beam finite element with nodes offset to either the top or bottom side has been developed. The delaminated beam is considered as two sublaminates above and below the plane of delamination, and these are modeled by offset beam finite elements. An expression for the J-integral in terms of force and moment resultants in sublaminates connected to the crack tip is derived. From the J-integral two more methods of computing the strain energy release rate have been developed. In the crack tip force method, the strain energy release rate is expressed in terms of forces transmitted by the crack tip rigid element. The second method is similar to the crack closure method used in two-dimensional fracture problems. The effectiveness of the present method is illustrated by analyzing three composite test specimens widely used to measure fracture toughness.

1. INTRODUCTION

The subjects of stress analysis of delaminations, analytical and numerical methods for predicting the mechanical behavior of delaminated structures, and inspection methods for characterizing delaminations and debonding have received considerable attention in recent years [1]. An analytical prediction methodology for delamination growth is important for determining the useful life and frequency of inspection of any delaminated structure. The general principles in the analysis of delaminations have been (a) estimation of a fracture parameter under the given loading conditions, and (b) comparison of that with a critical parameter for the particular material system and laminate configuration measured, using coupons with implanted delaminations. The strain energy release rate has been accepted as the standard fracture parameter not only because it is convenient, but also because it is based on a sound energy balance principle.

Effective numerical or analytical methods are necessary for the analysis of delaminations in both a laminated structural element and test specimens used to measure fracture toughness. A fully three-dimensional stress analysis, e.g. [2], will be prohibitively expensive, and may not be necessary, at least during the initial stages of design and analysis. Analytical methods based on laminated plate theories have also been developed [3]. Finite element methods are popular for their ability to model complex shapes and loading conditions. In the present study a novel finite element is proposed for the analysis of delaminations, and its effectiveness is illustrated by using the method to analyze some composite beam specimens widely used to measure fracture toughness.

In the present study we assume that the delamination will continue to grow in the same plane. The laminate is divided into two sublaminates, one below and one above the plane of delamination. The sublaminates are modeled by finite elements with nodes offset to the top or bottom. In the uncracked portion the nodes corresponding to the top and bottom sublaminates are connected by rigid elements that ensure continuity of displacements and rotation at the plane of delamination. In the cracked portion the nodes of top and bottom sublaminates are connected by gap elements that will be effective only when contact occurs. We assume that there is no friction against sliding of the sublaminates, if they are in contact. The concept of offsetting the nodes has been in use to join a beam element with some other type of element, for instance, a plate element [4]. Modifying the conventional beam element stiffness matrix to account for offset results in error due to incompatible displacement fields [5].

In the present study we develop a shear deformable beam finite element with nodes offset to the bottom or top side of the beam. This formulation introduces new stiffness terms b_{11} and d_{11}, which are different from the conventional stiffness terms B_{11} and D_{11}. An expression for the J-integral in terms of the newly defined force and moment resultants is derived. From the expression for the J-integral two new methods of computing G, the strain energy release rate, are derived. Both methods are convenient in the sense that the necessary quantities are degrees of freedom in the finite element model, and hence are part of the solution. In the first method, the crack tip force method, G is computed from the forces in the crack tip rigid element. Physically, this means that the crack tip element will break when the set of forces transmitted by that element exceeds a certain limit. The second method is analogous to the virtual crack closure method. The results are compared with G

computed using analytical methods, and the agreement is found to be excellent.

2. LAMINATED BEAM EQUATIONS

In this section we derive the relevant equations for a laminate beam which is situated just above the reference plane (x–y-plane). The procedure is very similar to that for conventional composite laminate equations, where the x–y-plane is the midplane of the laminate and shear deformation is also considered. The in-plane and transverse displacements are assumed to be of the form

$$u(x, z) = u_0(x) + z\psi(x) \tag{1}$$

and

$$w(x, z) = w(x) \tag{2}$$

where $u_0(x)$ is the axial displacement of points in the x–y-plane, and $\psi(x)$ is the rotation about the y-axis. The transverse displacements, $w(x)$, are assumed to be constant through the thickness of the laminate. The strains can be derived as

$$\epsilon_{xx} \equiv u_{,x} = u_{0,x} + z\psi_{,x} \tag{3}$$

and

$$\gamma_{xz} \equiv u_{,z} + w_{,x} = \psi + w_{,x}. \tag{4}$$

In eqns (3) and (4), a comma denotes partial differentiation with respect to the subscripted variable.

The force and moment resultants are defined as

$$\mathbf{F}^{\mathbf{T}} = \lfloor P, M, V \rfloor = \int_0^h \lfloor \sigma_{xx}, z\sigma_{xx}, \tau_{zx} \rfloor \, dz, \tag{5}$$

where h is the beam thickness. In eqn (5), and throughout the paper, boldface letters denote matrices, and a superscript $\mathbf{T}$ denotes the transpose of a matrix. We will assume that there is no bending–twisting or extension–twisting coupling in the laminate. Assuming a state of plane strain parallel to the x–z-plane, the stress–strain relations [6] for a layer are

$$\sigma_{xx} = \bar{Q}_{11}\epsilon_{xx} \tag{6}$$

and

$$\tau_{xz} = \bar{Q}_{55}\gamma_{xz}. \tag{7}$$

From eqns (3)–(7), we obtain

$$\mathbf{F} = \mathbf{se}, \tag{8}$$

where the notations

$$\mathbf{s} = \begin{bmatrix} a_{11} & b_{11} & 0 \\ b_{11} & d_{11} & 0 \\ 0 & 0 & a_{55} \end{bmatrix}$$

and

$$\mathbf{e}^{\mathbf{T}} = \lfloor \epsilon_{xx}, \kappa_{xx}, \gamma_{xz} \rfloor$$

are used. The stiffness coefficients of the laminate are defined as

$$\lfloor a_{11}, b_{11}, d_{11}, a_{55} \rfloor = \int_0^h \lfloor \bar{Q}_{11}, z\bar{Q}_{11}, z^2\bar{Q}_{11}, \kappa\bar{Q}_{55} \rfloor \, dz. \tag{9}$$

In the above relations $\kappa_{xx} = \psi_{,x}$ is the beam curvature, and the shear correction factor, κ, may be assumed as 5/6. It may be noted that for a given laminate the stiffness coefficients a_{11} and a_{55} will be equal to A_{11} and A_{55} of the conventional laminated plate theory, but b_{11} and d_{11} will be different from B_{11} and D_{11}. The above relations are for a laminate which is above the x–y-plane. For a laminate below the x–y-plane, the lower and upper limits of integration in eqns (5) and (9) will be $-h$ and 0 respectively. For two identical laminates situated symmetrically about the x–y-plane, a_{11}, a_{55} and d_{11} terms will be the same, but b_{11} will differ only in sign.

In the following an expression for strain energy per unit length of the beam will be derived. Denoting the strain energy density by W and strain energy per unit length of the laminate by U,

$$W = (1/2)(\sigma_{xx}\epsilon_{xx} + \tau_{xz}\gamma_{xz}) \tag{10}$$

and

$$U = \int_0^h W \, dz. \tag{11}$$

Substituting in eqn (10) the stress–strain relations (6) and (7), and the strain–displacement relations (3) and (4), and performing the integration in eqn (11), we obtain

$$U = (1/2)\mathbf{e}^{\mathbf{T}}\mathbf{se}. \tag{12}$$

An alternative expression for U can be obtained as follows. Let $\mathbf{c} = \mathbf{s}^{-1}$. Then $\mathbf{e} = \mathbf{s}^{-1}\mathbf{F} = \mathbf{cF}$. Substituting in eqn (12) we obtain

$$U = (1/2)\mathbf{F}^{\mathbf{T}}\mathbf{cF}. \tag{13}$$

3. BEAM FINITE ELEMENT WITH OFFSET NODES

In this section a beam finite element with nodes offset either to the top or bottom side of the beam is developed. The beam element has three nodes as shown in Fig. 1. The two extreme nodes have three degrees of freedom each, u, ψ, and w respectively. At the middle node only w displacement is defined. The displacements are interpolated as

$$u(x) = u_1 N_1(x) + u_2 N_2(x) \tag{14}$$

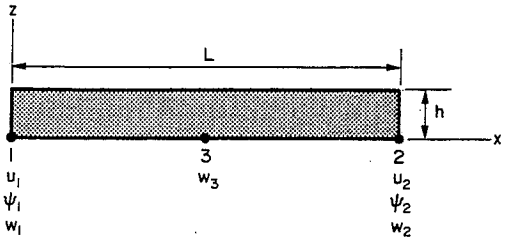

Fig. 1. Beam finite element with nodes offset to bottom side.

$$\psi(x) = \psi_1 N_1(x) + \psi_2 N_2(x) \tag{15}$$

and

$$w(x) = w_1 N_1(x) N_3(x) - w_2 N_2(x) N_3(x) + 4w_3 N_1(x) N_2(x). \tag{16}$$

The interpolation functions are defined as $N_1(x) = (1 - x/L)$, $N_2(x) = x/L$, and $N_3(x) = (1 - 2x/L)$, where L is the element length. The strain energy in the beam element is given by

$$U_e = \int_0^L U \, dx. \tag{17}$$

Substituting the assumed displacements (14)–(16) in eqn (12), and using eqns (3) and (4), we obtain

$$U_e = (1/2)\mathbf{q}^T \mathbf{k}' \mathbf{q}, \tag{18}$$

where $\mathbf{k}'$ is the 7×7 stiffness matrix and $\mathbf{q}$ is the vector of nodal displacements. The stiffness matrix is given in Appendix A. Although one can work with the 7×7 stiffness matrix, it has been found to be more efficient to apply static condensation to remove the central node. The resulting 6×6 stiffness matrix $\mathbf{k}$ is also given in Appendix A.

It may be noted that the present finite element gives the exact solution for a couple or an axial force applied at the tip of a cantilever beam. Hence the performance of the finite element was evaluated by considering an orthotropic cantilever beam of length l and unit width subjected to a transverse end load. The beam material principal directions 1–2–3 coincide with the x–y–z-axes. In that case $\bar{Q}_{11} = Q_{11} = E_1/(1 - \nu_{12}\nu_{21})$, and $\bar{Q}_{55} = Q_{55} = G_{13}$. To bring in the effect of shear deformations, the shear modulus G_{13} of the beam material was assumed to be equal to $E_1/80$. The tip displacements for various l/h ratios are shown in Fig. 2. The displacement results are normalized with respect to the Bernoulli–Euler beam tip deflection given by $4Pl^3/3d_{11}$. It may be seen that with three elements the present finite element gives exact solution in the wide range of $0.1 < l/h < 1000$. It is instructive to note here that for very short cantilever beams, e.g. $l/h < 1$, one element solution for tip deflections, $\mathbf{q}_{tip}$, is found to be

$$\mathbf{q}_{tip} = l\mathbf{c}\mathbf{R}, \tag{19}$$

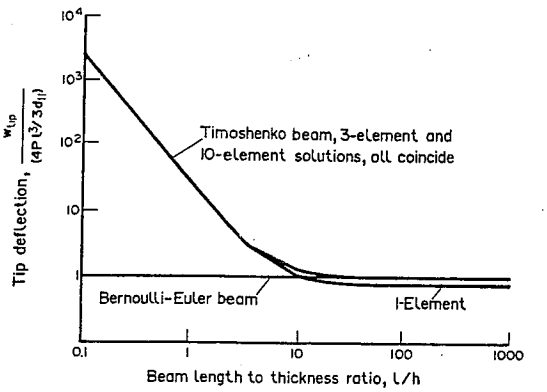

Fig. 2. Tip deflection of cantilever beams for various l/h ratios.

where $\mathbf{R}$ is the vector consisting of axial force, couple, and transverse force applied at the tip of the beam. This result will be used later to derive a virtual crack closure formula for strain energy release rate in delaminated beams.

4. MODELING DELAMINATIONS

In modeling delaminations in a composite beam, we assume that the given laminate consists of two sub-laminates, one above and one below the delamination plane (x–y-plane), as shown in Fig. 3. Further, we assume that the delamination plane is the weakest and the crack will propagate parallel to the x–y-plane. Thus the possibilities of crack branching are ignored. Beam finite elements with nodes offset to the bottom and top are used to model the top and bottom sublaminates respectively. In the uncracked portion of the beam the nodes of the top and bottom elements will be connected by rigid elements to ensure continuity of displacements and rotation between the top and bottom sublaminates. If one is interested only in the impending delamination growth, then it will be sufficient to connect the pair of crack tip nodes (Nodes 1 and 2) by a rigid element, and have common nodes (for example, Node 5 in Fig. 3) for the top and bottom elements ahead of the crack tip. The rigid element has nine degrees of freedom. Apart from the three displacements at each node, the three generalized forces the rigid element transmits are also considered as unknown degrees of freedom. Thus, the degrees of freedom of the rigid element are u_1, ψ_1, w_1, u_2, ψ_2, w_2, and F_{xr}, M_{yr}, and F_{zr}. The last three terms are the forces transmitted by the rigid element.

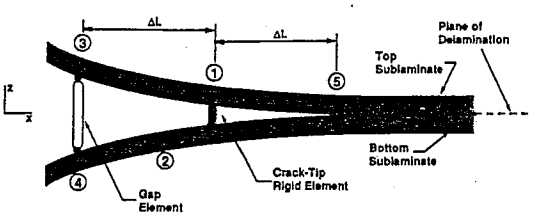

Fig. 3. Finite element model of delamination.

The constraint equations corresponding to the rigid element can be written as

$$\begin{Bmatrix} \mathbf{F}_1 \\ \mathbf{F}_2 \\ \mathbf{0} \end{Bmatrix} = \begin{bmatrix} \mathbf{0}_3 & \mathbf{0}_3 & -\mathbf{I}_3 \\ \mathbf{0}_3 & \mathbf{0}_3 & \mathbf{I}_3 \\ -\mathbf{I}_3 & \mathbf{I}_3 & \mathbf{0}_3 \end{bmatrix} \begin{Bmatrix} \mathbf{q}_1 \\ \mathbf{q}_2 \\ \mathbf{F}_r \end{Bmatrix}, \tag{20}$$

where $\mathbf{F}_1$ and $\mathbf{F}_2$ are the nodal force vectors at Nodes 1 and 2, $\mathbf{q}_1$ and $\mathbf{q}_2$ are the vectors of nodal displacements, $\mathbf{F}_r$ is the vector of forces transmitted by the rigid element, $\mathbf{I}_3$ is the 3×3 identity matrix, and $\mathbf{0}_3$ is the 3×3 null matrix. The stiffness matrix in eqn (20) can be multiplied by a suitable factor, say k_f, so that it will be of the same order of magnitude as that of the beam stiffness matrix. Thus eqn (20) becomes

$$\begin{Bmatrix} \mathbf{F}_1 \\ \mathbf{F}_2 \\ \mathbf{0} \end{Bmatrix} = \begin{bmatrix} \mathbf{O}_3 & \mathbf{0}_3 & -k_f\mathbf{I}_3 \\ \mathbf{O}_3 & \mathbf{0}_3 & k_f\mathbf{I}_3 \\ -k_f\mathbf{I}_3 & k_f\mathbf{I}_3 & \mathbf{0}_3 \end{bmatrix} \begin{Bmatrix} \mathbf{q}_1 \\ \mathbf{q}_2 \\ \mathbf{F}_r/k_f \end{Bmatrix}. \tag{21}$$

Gap elements are used to connect the top and bottom sublaminates in the cracked portion as shown in Fig. 3. The gap elements are rigid elements that transfer only transverse compressive forces and will be effective only when the crack closes. In the present study we assume that there is no frictional resistance against sliding of the sublaminates. The constraint equations of a gap element will be similar to that given in eqn (21), but of size 3×3 as shown below:

$$\begin{Bmatrix} F_{z1} \\ F_{z2} \\ 0 \end{Bmatrix} = \begin{bmatrix} 0 & 0 & -k_f \\ 0 & 0 & k_f \\ -k_f & k_f & 0 \end{bmatrix} \begin{Bmatrix} w_1 \\ w_2 \\ F_c/k_f \end{Bmatrix}. \tag{22}$$

In eqn (22) F_{z1} and F_{z2} are the nodal forces, w_1 and w_2 are the nodal displacements and F_c is the contact force transmitted. F_c is negative when the gap element is under compression.

5. COMPUTATION OF STRAIN ENERGY RELEASE RATE

In this section we will discuss three methods of computing G, the strain energy release rate. We will derive an expression for the J-integral, which is identically equal to G, in terms of the force and moment resultants in the sublaminates connecting the crack tip. Based on the expression for J, we will develop two more methods to compute G from the finite element results.

5.1. *J-Integral*

Considering a zero volume path surrounding the crack tip as shown in Fig. 4(a), an expression for the J-integral is given by [7]

$$J = \int_\Gamma [Wn_x - n_x(\sigma_{xx}u_{,x} + \tau_{xz}w_{,x}) - n_z\tau_{xz}u_{,x}]\,ds. \tag{23}$$

The path Γ consists of four segments, one in each sublaminate behind and ahead of the crack tip, as shown in Fig. 4(b). For the path Γ_1, $n_x = -1$ and $ds = -dz$, and the J-integral takes the form

$$J^{(1)} = -\int_{-h}^{0} (W - \sigma_{xx}u_{,x} - \tau_{xz}w_{,x})\,dz. \tag{24}$$

Substituting for the strain energy density from eqn (10), and using eqns (3), (4), (6), (7) and (11), we obtain

$$J^{(1)} = U^{(1)} - V_1\psi_1, \tag{25}$$

where $U^{(1)}$ and V_1 are the strain energy per unit length and shear force resultant respectively in sublaminate

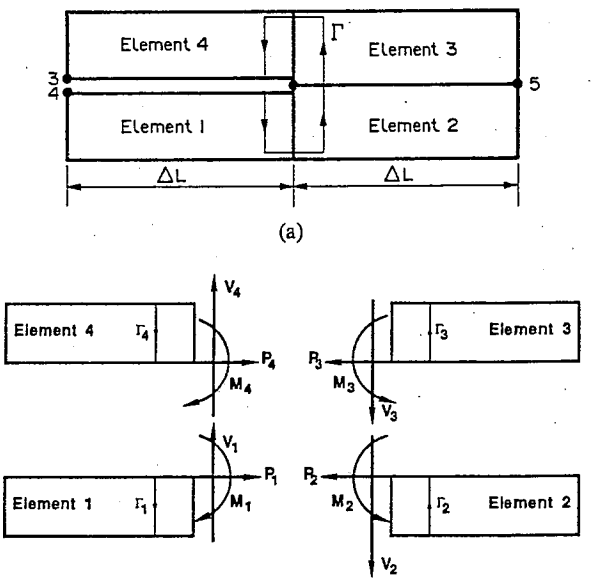

Fig. 4. (a) Zero-volume path for J-integral. (b) Forces in crack-tip elements.

1 just behind the crack tip. ψ_t is the rotation at the crack tip, which is same for all the four sublaminates connected at the crack tip. Similarly, for the paths Γ_2, Γ_3, and Γ_4, we obtain

$$J^{(2)} = -U^{(2)} + V_2\psi_t,$$

$$J^{(3)} = -U^{(3)} + V_3\psi_t,$$

$$J^{(4)} = U^{(4)} - V_4\psi_t,$$

and

$$J = J^{(1)} + J^{(2)} + J^{(3)} + J^{(4)}. \tag{26}$$

Considering the equilibrium of forces in the z-direction at the crack tip,

$$V_1 + V_4 = V_2 + V_3. \tag{27}$$

Then eqn (26) becomes

$$J = U^{(1)} + U^{(4)} - U^{(2)} - U^{(3)}. \tag{28}$$

Substituting for the strain energy density U from eqn (13)

$$J = (1/2)(\mathbf{F}_1^T\mathbf{c}_b\mathbf{F}_1 - \mathbf{F}_2^T\mathbf{c}_b\mathbf{F}_2 - \mathbf{F}_3^T\mathbf{c}_t\mathbf{F}_3 + \mathbf{F}_4^T\mathbf{c}_t\mathbf{F}_4). \tag{29}$$

In the above expression $\mathbf{F}_i$ denotes the force resultants in the ith sublaminate at the crack tip; $\mathbf{c}_b$ and $\mathbf{c}_t$ denote the $\mathbf{c}$ matrix of the bottom and top sublaminates respectively. The force and moment resultants can be obtained from the finite element results, and J can be evaluated using eqn (29).

5.2. *Crack tip force method*

A much more convenient method of computing G can be derived from eqn (29). Considering the sublaminates 2 and 3, relations between the force resultants $\mathbf{F}_2$, $\mathbf{F}_3$ and deformations $\mathbf{e}_2$, $\mathbf{e}_3$ can be written as $\mathbf{c}_b\mathbf{F}_2 = \mathbf{e}_2$, and $\mathbf{c}_t\mathbf{F}_3 = \mathbf{e}_3$. However, sublaminates 2 and 3 are integral and hence $\mathbf{e}_2 = \mathbf{e}_3$. We thus obtain the relation

$$\mathbf{c}_b\mathbf{F}_2 = \mathbf{c}_t\mathbf{F}_3. \tag{30}$$

Substituting eqn (30) in eqn (29), and also using the equilibrium relations $(\mathbf{F}_1 + \mathbf{F}_4) = (\mathbf{F}_2 + \mathbf{F}_3)$, we obtain

$$J = G = (1/2)(\mathbf{F}_1 - \mathbf{F}_2)^T(\mathbf{c}_t + \mathbf{c}_b)(\mathbf{F}_1 - \mathbf{F}_2). \tag{31}$$

Actually $(\mathbf{F}_1 - \mathbf{F}_2)$ is the force transmitted by the rigid element between the bottom and top crack tip nodes. Thus, G can be written as

$$G = (1/2)\mathbf{F}_r^T(\mathbf{c}_t + \mathbf{c}_b)\mathbf{F}_r, \tag{32}$$

where $\mathbf{F}_r$ is the vector of forces in the crack tip rigid element. The above equation provides a convenient method of calculating G, as the components of $\mathbf{F}_r$ are degrees of freedom of the rigid element connecting the crack tips, and they are part of the finite element solution.

At this point, some similarities between the crack tip force method and the foundation spring model [8] can be observed. In the foundation spring model, the uncracked portions of the beam are assumed to be connected by springs. The energy in the crack tip springs is considered as the energy of fracture, and the springs are ruptured when the energy reaches a critical level. Such foundation parameters have not yet been calculated for composite laminates, but the expression in eqn (32) provides some guidelines for such an approach. Usually, the foundation springs are very stiff, and the forces in the crack tip spring can be assumed to be equal to that in the crack tip rigid element. Then from eqn (32) it may be seen that for a given strain energy, the compliance term $(\mathbf{c}_t + \mathbf{c}_b)$ can be considered as the foundation spring compliance $\mathbf{c}_s$. It may be noted that the rotational and shear springs are coupled in this case. The inverse of the compliance matrix $\mathbf{c}_s$ is the foundation spring stiffness matrix $\mathbf{s}_s$. For a homogeneous orthotropic beam of thickness $2h$ with a midplane crack, $\mathbf{s}_s$ is diagonal. Approximating Q_{11} by E_1 and Q_{55} by G_{13}, the diagonal terms become $E_1h/8$, $E_1h^3/24$, and $G_{13}h/2$, and they represent the shear, rotational and extensional stiffness of the foundation respectively.

5.3. *Crack closure method*

Referring to Fig. 3, as the crack propagates, the crack tip Nodes 1 and 2 separate, and the crack tip moves to Node 5. The relative displacements of Nodes 1 and 2 can be computed by applying the pair of self-equilibrating forces $\mathbf{F}_r$ and $-\mathbf{F}_r$ at Nodes 1 and 2. If, ΔL, lengths of finite elements just ahead of the crack tip, are sufficiently small, then the displacements of Nodes 1 and 2 are the tip displacements of a cantilever beam of length ΔL, and can be obtained using eqn (19). Defining the crack opening displacements as $\Delta\mathbf{q}_1$ and $\Delta\mathbf{q}_2$ we obtain from eqn (19)

$$\Delta\mathbf{q}_1 = \Delta L\ \mathbf{c}_t\mathbf{F}_r, \quad \text{and} \quad \Delta\mathbf{q}_2 = -\Delta L\ \mathbf{c}_b\mathbf{F}_r. \tag{33}$$

Substituting eqn (33) in eqn (32) we obtain

$$G = (1/2\ \Delta L)\mathbf{F}_r^T(\Delta\mathbf{q}_1 - \Delta\mathbf{q}_2), \tag{34}$$

which is analogous to the virtual crack closure method used in two-dimensional fracture problems [9]. If sufficiently small finite elements are used, and if the lengths of elements behind the crack tip are also ΔL, then $(\Delta\mathbf{q}_1 - \Delta\mathbf{q}_2)$ will be approximately equal to the difference in displacements of Nodes 3 and 4 behind the crack tip before the impending propagation. Then G can be computed from

$$G = (1/2\ \Delta L)\mathbf{F}_r^T(\mathbf{q}_3 - \mathbf{q}_4). \tag{35}$$

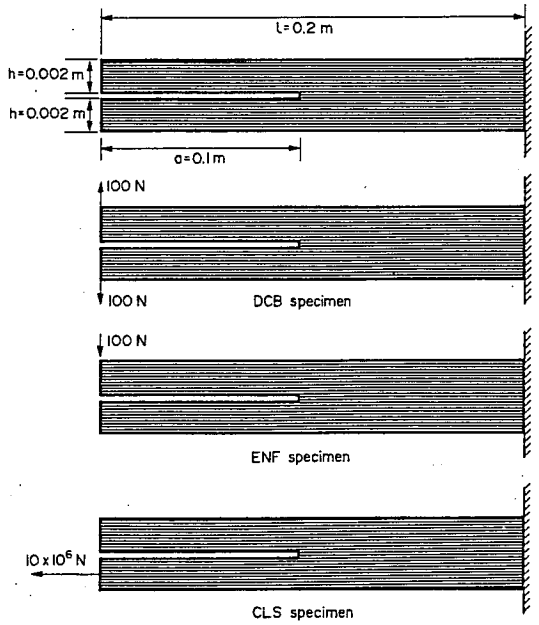

Fig. 5. Specimen dimensions and loads.

6. NUMERICAL EXAMPLES

To illustrate the effectiveness of the proposed method, three widely used composite specimens are considered: (1) the double cantilever beam (DCB); (2) the end notch flexure specimen (ENF); and (3) the cracked lap shear specimen (CLS). In fact, all three specimens have the same geometry except for the loading conditions. The specimen considered is an orthotropic beam with a midplane crack through half of its length. The specimen dimensions and the loads are shown in Fig. 5. The width in the y-direction is assumed to be unity. The properties of the orthotropic materal are $E_1 = 200$ GPa, $E_2 = 5$ GPa, $G_{13} = 2.4$ GPa, and $\nu_{12} = 0.28$. For a laminate of thickness 0.002 m, the laminate stiffness coefficients are: $a_{11} = 408 \times 10^6$ N/m, $b_{11} = 0.408 \times 10^6$ N, $d_{11} = 544$ Nm, and $a_{55} = 4 \times 10^6$ N/m. The length of the finite elements connecting the crack tip was varied from 10^{-3} to 10^{-5} m. The element length in other parts of the beam was about 0.005 m. Gap elements were used in the delaminated portion of the ENF specimen. The applied load is 100 N for the DCB and ENF specimens, and 10×10^6 N for the CLS specimen. In the case of the CLS specimen, two types of boundary conditions are considered. In CLS/1, the lateral deflection and rotation of the bottom sublaminate at the point of application of load are not constrained. In the second case (CLS/2 specimen), the lateral deflection and rotation at the tip are set to zero, which is a better representation of boundary conditions of test specimens. In the CLS/1 specimen, the resultant of the applied axial force is assumed to be at the center of the bottom laminate. In the present finite element model this force, F, has to be resolved into a force acting at the node at the top side of the laminate and a positive couple equal to $Fh/2$, where h is the sublaminate thickness.

The results are presented in Table 1. The finite element method was used to compute the force resultants in the four crack tip beam elements, the forces in the crack tip rigid element, and the displacements of the two nodes immediately behind the crack tip. The strain energy release rates G_A, G_J, G_T, and G_C were computed using respectively analytical methods (see Appendix B), the J-integral [eqn (29)], crack tip force method [eqn (32)], and crack closure method [eqn (35)]. The shear force F_{xr}, bending moment M_{yr} and transverse normal force F_{zr} transmitted by the crack tip rigid element are also given in Table 1. The agreement in G values obtained using various methods is excellent. The ENF specimen needed a finer mesh near the crack tip to obtain the exact solution. In the case of the CLS specimens, there is a significant difference in G values between CLS/1 and CLS/2. The G for CLS/2 is about five times that of CLS/1. The shear force transmitted by the crack tip rigid element in CLS/2 is about twice that in CLS/1 specimen. Further significant amounts of transverse force and bending moment are also transmitted by the crack tip rigid elements in the CLS/2 specimen.

7. CONCLUDING REMARKS

A laminated shear deformable beam finite element with nodes offset to either top or bottom has been developed. This element is used to model the sublaminates above and below the plane of delamination. A rigid element is used to connect the crack tip nodes. The strain energy release rate can be calculated using

Table 1. Strain energy release rates and crack tip forces in various specimens

Specimen	G_A (N/m)	G_J (N/m)	G_T (N/m)	G_C (N/m)	F_{xr} (N)	M_{yr} (Nm)	F_{zr} (N)
DCB $\Delta L = 10^{-3}$ m	0.7378	0.7378	0.7378	0.7378	0	10	100
CLS/1 $\Delta L = 10^{-3}$ m	0.1532	0.1532	0.1532	0.1532	1.25×10^6	0	0
CLS/2 $\Delta L = 10^{-3}$ m	—	0.7700	0.7701	0.7677	2.44×10^6	1586	26,492
ENF $\Delta L = 10^{-3}$ m	0.1379	0.1379	0.1379	0.1379	3769	0	0
ENF $\Delta L = 10^{-5}$ m	0.1379	0.1379	0.1379	0.1379	3750	0	0

one of the three methods: J-intergal, crack tip force method, or crack closure method. The last two methods are convenient as the crack tip forces and displacements are part of the finite element solution. There are several advantages to the present formulation. The finite element method can be used to model any type of geometry and loading condition (the CLS/2 specimen is a good example). Renumbering of nodes and elements as the crack propagates can be avoided. Friction between the contacting surfaces of sublaminates can be modeled by using appropriate friction elements between the top and bottom node, and using incremental loading. If one is interested in using the foundation spring model, appropriate foundation springs can be used in place of the rigid elements in the uncracked portion of the beam. The present method will be very useful in studying dynamic delamination propagation problems [10, 11], as the energy release rate can be calculated using the crack closure method. Further, the present method can be extended to problems of sublaminate buckling and delaminations in composite plates.

Acknowledgements—This research was supported by a DARPA grant to the University of Florida under the program Innovative Processing of Composites for Ultra High Temperature Applications. The author thanks Mr Shoufeng Hu, graduate student, for his help in computations.

REFERENCES

1. W. S. Johnson (Editor), *Delamination and Debonding of Materials*, *ASTM STP* 876. American Society for Testing and Materials, Philadelphia, PA (1985).
2. A. Y. Kuo and S. S. Wang, A dynamic hybrid finite-element analysis for interfacial cracks in composites. In *Delamination and Debonding of Materials*, *ASTM STP* 876 (Edited by W. S. Johnson), pp. 5–34. American Society for Testing and Materials, Philadelphia, PA (1985).
3. P. Sriram and E. A. Armanios, Fracture analysis of local delaminations in laminated composites. AIAA Paper No. 89-1400-CP. Collection of Technical Papers presented at the 30th SDM Conf., Part 4, pp. 2098–2108 (1989).
4. R. D. Cook, D. S. Malkus and M. E. Plesha, *Concepts and Applications of Finite Element Analysis*. John Wiley, New York (1989).
5. A. K. Gupta and P. S. Ma, Error in eccentric beam formulation. *Int. J. Numer. Meth. Engng* **11**, 1473–1483 (1977).
6. R. M. Jones, *Mechanics of Composite Materials*. Scripta Book Co., Washington, DC (1975).
7. M. F. Kanninen and C. H. Popelar, *Advances Fracture Mechanics*. Oxford University Press, New York (1985).
8. M. F. Kanninen, A dynamic analysis of unstable crack propagation and arrest in the DCB test specimen. *Int. J. Fract.* **10**, 415–430 (1974).
9. E. F. Rybicki and M. F. Kanninen. A finite element calculation of stress intensity factors by a modified crack closure integral. *Engng Fract. Mech.* **9**, 931–938 (1977).
10. S. Hu, B. V. Sankar and C. T. Sun, A finite element study of dynamic delamination growth in composite laminates. AIAA Paper No. 89-1301-CP. Collection of Technical Papers presented at the 30th SDM Conf., Part 3, pp. 1250–1255 (1989).
11. J. E. Grady and C. T. Sun, Dynamic delamination propagation in a graphite/epoxy laminate. In *Composite Materials: Fatigue and Fracture*, *ASTM STP* 907, pp. 5–31. American Society for Testing and Materials, Philadelphia, PA (1986).
12. R. L. Ramkumar and J. D. Whitcomb, Characterization of mode I and mixed-mode delamination growth in T300/5208 graphite/epoxy. In *Delamination and Debonding of Materials*, *ASTM STP* 876 (Edited by W. S. Johnson), pp. 315–335. American Society for Testing and Materials, Philadelphia, PA (1985).

APPENDIX A

The non-zero coefficients of the 7×7 symmetric stiffness matrix $\mathbf{k}'$ are given below. The degrees of freedom in the appropriate order are u_1, ψ_1, w_1, u_2, ψ_2, w_2, and w_3 (see Fig. 1). The element length is L, and the width in the y-direction is assumed to be unity. The stiffness matrix is derived for a laminate situated above the x–y-plane, i.e. z is positive everywhere in the laminate. As noted in Sec. 2, for a laminate below the x–y-plane, the only difference is in the sign of b_{11}. Alternatively, a coordinate transformation can be used to obtain the stiffness matrix in global coordinates:

$$k'_{11}=a_{11}/L,\quad k'_{12}=b_{11}/L,\quad k'_{14}=-a_{11}/L,\quad k'_{15}=-b_{11}L,$$

$$k'_{22}=d_{11}/L+a_{55}L/3,\quad k'_{23}=-5a_{55}/6,\quad k'_{24}=-b_{11}/L,$$

$$k'_{25}=-d_{11}/L+a_{55}L/6,$$

$$k'_{26}=a_{55}/6,\quad k'_{27}=2a_{55}/3,\quad k'_{33}=7a_{55}/3L,\quad k'_{35}=-a_{55}/6,$$

$$k'_{36}=a_{55}/3L,\quad k'_{37}=-8a_{55}/3L,\quad k'_{44}=a_{11}/L,\quad k'_{45}=b_{11}/L,$$

$$k'_{55}=k'_{22},\quad k'_{56}=5a_{55}/6,\quad k'_{57}=-2a_{55}/3,$$

$$k'_{66}=7a_{55}/3L,\quad k'_{67}=-8a_{55}/3L,\quad k'_{77}=16a_{55}/3L.$$

After removing the w_3 degree of freedom by using static condensation, we obtain the 6×6 stiffness matrix $\mathbf{k}$ as given below. The non-zero coefficients of $\mathbf{k}$ are

$$k_{11}=a_{11}/L,\quad k_{12}=b_{11}/L,\quad k_{14}=-k_{11},$$

$$k_{15}=-k_{12},\quad k_{22}=d_{11}/L+a_{55}L/4,$$

$$k_{23}=-a_{55}/2,\quad k_{24}=k_{15},\quad k_{25}=-d_{11}/L+a_{55}L/4,$$

$$k_{26}=a_{55}/2,\quad k_{33}=a_{55}/L,$$

$$k_{35}=k_{23},\quad k_{36}=-k_{33},\quad k_{44}=k_{11},\quad k_{45}=k_{12},$$

$$k_{55}=k_{22},\quad k_{56}=k_{26},\quad k_{66}=k_{33}.$$

APPENDIX B

In this section a brief description of the analytical method used to compute the strain energy release rate G_A is given. The elastic strain energy U_s in the specimens considered in Sec. 6 are in general given by

$$U_s=(1/2)Pq, \tag{B1}$$

where P is the applied load and q is the corresponding displacement. For the constant load case the strain energy release rate is simply the derivative of the strain energy U_s with respect to the crack length a. Thus

$$G=\mathrm{d}U_s/\mathrm{d}a=(1/2)P\,\mathrm{d}q/\mathrm{d}a. \tag{B2}$$

The displacements q and strain energy release rate G for the three specimens considered are given below. It may be mentioned again that in the following expressions $d_{11} = Q_{11}h^3/3$, which is different from D_{11}. For the DCB specimen the strain energy has to be doubled.

$$q_{DCB} = 4Pa^3/3d_{11} + Pa/a_{55} \tag{B3}$$

$$G_{DCB} = 4P^2a^2/d_{11} + P^2/a_{55} \tag{B4}$$

$$q_{ENF} = Pa^3/2d_{11} + Pl^3/6d_{11} + Pl/2a_{55} \tag{B5}$$

$$G_{ENF} = 3Pa^2/4d_{11}. \tag{B6}$$

For the CLS/1 specimen, assuming that the force P is applied at the center of the bottom sublaminate,

$$q_{CLS1} = P(l + a)/2a_{11} + P(l - a)h^2/8d_{11} \tag{B7}$$

$$G_{CLS1} = P^2/4a_{11} - P^2h^2/16d_{11}. \tag{B8}$$

In eqn (B8) the second term on the right-hand side represents the bending effect due to eccentric loading. In [12], this term was considered to be small and was neglected. For a homogeneous orthotropic beam $d_{11} = a_{11}h^2/3$. Substituting in eqn (B8) we obtain $G_{CLS1} = P^2/16a_{11}$, which is only one-fourth of G obtained ignoring the bending effect.

The analtyical solution for CLS/2 is not given here, but the finite element results given in Table 1 show that the G for CLS/2 is about five times that of CLS/1.